# Electronic structure and small polaron hole transport of copper aluminate

B. J. Ingram and T. O. Mason
*Department of Materials Science and Engineering, Materials Research Center, Northwestern University, Evanston, Illinois 60208*

R. Asahi
*Toyota Central R&D Laboratories, INC, Nagakute, Aichi 480-1192, Japan*

K. T. Park* and A. J. Freeman
*Department of Physics and Astronomy, Materials Research Center, Northwestern University, Evanston, Illinois 60208*
(Received 5 March 2001; published 28 September 2001)

High-temperature electrical property measurements (electrical conductivity, thermoelectric coefficient) on polycrystalline $CuAlO_2$ exhibited characteristic small polaron features, i.e., low mobilities (0.1–0.4 $cm^2/V\,s$) and an activation energy of ~0.14 eV. The thermopower was *p* type (~440 $\mu V/K$) and roughly temperature independent. The local-density full-potential linearized augmented-plane-wave method was used to calculate the band structure, densities of states, and optical properties (within the electric-dipole approximation) in order to account for the unique electronic and optical properties of this potential transparent conducting oxide.

DOI: 10.1103/PhysRevB.64.155114 PACS number(s): 71.38.Ht, 72.80.Jc, 78.20.Bh

## I. INTRODUCTION

The development of a high-figure-of-merit *p*-type transparent conducting oxide (TCO) would enable improved flat-panel displays, ultraviolet emitting diodes, heterojunctions for solar cells, and all-oxide (transparent) semiconductor devices such as diodes and transistors.[1–3] To date, however, reported *p*-type TCO's lack sufficient conductivity to match that of currently employed *n*-type TCO's ($\sigma > 10^3$ S/cm), whether due to insufficient carrier content, mobility, or both. The current study was undertaken to investigate the electronic structure and transport properties of $CuAlO_2$, the first of a family of delafossite-based *p*-type materials under development for TCO applications.[4]

$CuAlO_2$ crystallizes in the delafossite structure with a rhombohedral space group $R\bar{3}m$, which can be described by alternating layers of edge-shared $AlO_6$ octahedra and Cu close-packed planes and is shown in Fig. 1.[5–7] The copper is in linear coordination with oxygen and is in the $1+(d^{10})$ oxidation state. Metal oxides having the delafossite structure, with either rhombohedral $3R$ or hexagonal $2H$ stacking, exhibit behaviors ranging from insulating to semimetallic, depending upon the specific cations involved.[5–7]

Table I lists some of the room-temperature transport properties reported for $CuAlO_2$.[4,8–11] Except for the work of Benko and Koffyberg,[8] in which bulk polycrystalline specimens were employed, all the other measurements were performed on thin films. It is evident that reported conductivities are 3–6 orders of magnitude smaller than for conventional *n*-type TCO's. Carrier contents are typically 2–4 orders of magnitude smaller than for *n*-type TCO's, where $n > 10^{21}\,cm^{-3}$ and, except for the result of Kawazoe *et al.*,[4] mobilities are on the order of 1 $cm^2/V\,s$ or less. In contrast, the best *n*-type TCO's possess mobilities in the 10–100 $cm^2/V\,s$ range. Commensurate with the low carrier contents, thermoelectric coefficients are high, varying from 140 $\mu V/K$ (Ref. 10) to as large as 670 $\mu V/K$,[9] indicative of semiconducting behavior. Several of these studies reported variable-range hopping ($\ln \sigma \propto T^{-1/4}$) below ~200 K, but activated conductivity near room temperature with activation energies varying from 0.12 eV (Ref. 10) to 0.20 eV (Ref. 4) or 0.22 eV (Ref. 11). Similarly, Duan *et al.*[12] observed variable-range hopping over the range 80–300 K in $CuScO_{2+x}$, plus a room-temperature activation energy of 0.11 eV. Cava *et al.*[13] observed similar behavior in $CuYO_{2.51}$, i.e., conductivity $\sim 10^{-3}$ S/cm and an activation energy of ~0.23 eV near 300 K.

There is a question, however, concerning the role of grain boundaries in the room-temperature conductivity of the delafossites. Isawa *et al.*[14] synthesized a range of $CuMO_{2+x}$ delafossites ($M$ = Y, La, Pr, Nd, Sm, and Eu) in bulk polycrystalline form. Their room-temperature conductivities ranged from $10^{-3}$ S/cm ($A$ = Y) to on the order of 1 S/cm ($M$ = Sm, Nd, and Pr). At the same time, Isawa *et al.*[15] obtained metal-like room-temperature thermoelectric coeffi-

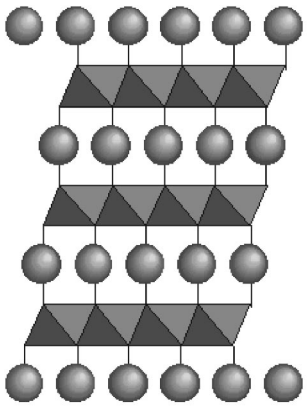

FIG. 1. Delafossite structure of the general formula $ABO_2$ comprised of alternating $BO_6$ edge-shared octahedral (shown as shaded polyhedra above) layers and two-dimensionally close-packed $A$ (shown as shaded spheres above) layers in linear coordination with oxygen.

 

cients ($S<30\,\mu$V/K) for all but the $M=$La ($S\sim40\,\mu$V/K) and $M=$Pr ($S\sim55\,\mu$V/K) delafossites. They suggested that the grain interiors were substantially doped, but that grain boundary barriers limited the electrical conductivity.

In the present work, high-temperature equilibrium electrical property measurements were undertaken on bulk polycrystalline $CuAlO_2$. The transition from variable-range hopping to conventional activated behavior appears to be essentially complete by room temperature.[4,11] Furthermore, it is well known that grain boundary barriers in electroceramics can often be overcome by increasing the temperature of the measurement.[16] Finally, high-temperature measurements allow for the specimen to be in point defect equilibrium with the ambient conditions, thereby facilitating analysis of the underlying carrier generation mechanism(s). Bulk specimens were chosen since they tend to be more robust than thin films at elevated temperatures.

To complement the high-temperature electrical property measurements, *ab initio* electronic structure calculations were also undertaken on $CuAlO_2$. Orgel originally proposed a *d-s* hybridized orbital model for Cu $d^{10}$ ions in linear twofold coordination (e.g., $Cu^+$ in $Cu_2O$).[17] Rogers *et al.*[18] attributed the anisotropic conductivity of the $CuAO_2$ delafossites to *d-s* hybridization of the $Cu^+$ ions. Ishiguro *et al.*[19] determined the electron density distribution in $CuAlO_2$ by single-crystal x-ray diffractometry and found substantial agreement with the Orgel hypothesis. Bradley and Cracknell[20] carried out scalar relativistic linearized muffin-tin orbital (LMTO) calculations within the atomic sphere approximation (ASA) on various delafossites, but did not consider $CuAlO_2$. Buljan *et al.*[21] performed Hartree-Fock (HF) calculations with *a posteriori* density functional corrections on $CuAO_2$ ($A=$Al, Ga, and Y) delafossites. Their work showed the top of the valence band to be dominated by Cu $3d$ states, with some contribution of Cu $4s$ ($s$-$d_{z^2}$ hybridization), in agreement with the Orgel hypothesis; however, band gaps of both the $2H$ and $3R$ $CuAlO_2$ polytypes were overestimated, as is typical for HF calculations, and electron charge density maps were not in good agreement with Ishiguro *et al.*[19]

Recently, Yanagi *et al.*[11] reported full-potential linearized augmented-plane-wave[22] (FLAPW) method results for $CuAlO_2$. They found the top of the valence band to be dominated by Cu-O bonding states, largely consistent with the results of Buljan *et al.*,[21] but with more reasonable optical gaps of 1.7 eV (indirect) and 2.8 eV (direct), the former in good agreement with the experimental results of Benko and Koffyberg.[8] In the present work, the FLAPW method was employed to calculate the band structure, densities of states (DOS), and optical properties (evaluated within the electric-dipole approximation), with special attention to resolving the origin of the unique (low-mobility) TCO character of $CuAlO_2$.

TABLE I. Room-temperature transport data for $CuAlO_2$.

| Source | $\sigma$ (S cm$^{-1}$) | $\mu$ (cm$^2$ V$^{-1}$ s$^{-1}$) | $p$ (cm$^{-3}$) | $Q$ ($\mu$V K$^{-1}$) |
|---|---|---|---|---|
| 8 | $1.7\times10^{-3}$ | $<0.1$ | | 670 |
| 4 | $9.5\times10^{-2}$ | 10.4 | $1.3\times10^{17}$ | 183 |
| | 1.0[a] | | | |
| 9 | $1.5\times10^{-2}$ | 1.3[b] | $7.0\times10^{16}$ | 140 |
| | $5\times10^{-2}$[a] | | $1.4\times10^{18}$[a] | |
| 10 | 2.0 | 0.16–0.5 | $1.8–2.6\times10^{19}$ | |
| 11 | $3.4\times10^{-1}$ | 0.13 | $2.7\times10^{19}$ | 214 |

[a]Claimed highest values.

[b]Calculated from other reported parameters.

## II. PROCEDURE

### A. Experiment

Bulk specimens of polycrystalline $CuAlO_2$ were produced by the solid-state reaction of high-purity oxides, CuO (Aldrich, 99.995%) and $Al_2O_3$ (Aldrich, 99.999%), which were ground together under acetone with a mortar and pestle in a 1:1 ratio. Once a homogeneous mixture was obtained, 12.5-mm-diam by 2–5-mm-thick pellets were cold pressed under 175 Mpa. The resulting pellets were surrounded by a small amount of sacrificial powder of the same nominal composition in order to prevent reaction between the pellet and the crucible. The pellets were then heated to 1100 °C in air for 24–36 h in high-purity alumina crucibles, whereafter they were air quenched to room temperature. Portions were subjected to phase analysis by Cu $K_\alpha$ x-ray diffraction (XRD, Rigaku). If impurity phases were detected, the pellets were reground and again pelletized, followed by one or two additional firings at 1100 °C in air, until they were phase pure by XRD.

The pellets were then cut by diamond saw into conductivity bars of approximate dimensions 10 mm $\times$5mm$\times$5 mm. Gold wires were tightly wrapped around the bars at approximately 1/3 and 2/3 positions along the bar, as described by Hong *et al.*[23] Gold was employed to eliminate the reaction between Pt-based metals and copper-based oxides at elevated temperatures.[23] A type-*S* (Pt-Pt/10% Rh) thermocouple was placed in contact with each gold lead and also in contact with gold foils at each end of the bar, the former serving as voltage leads and the latter as current leads for four-point dc conductivity measurements. In the measurement furnace, the specimen was positioned just off the hot zone at an appropriate point to generate a suitable thermal gradient along its length ($\sim$15–20 °C). The six thermoelectric emf's and corresponding temperature differences (between the six possible thermocouple combinations) were plotted to obtain the thermoelectric coefficient at a given average temperature. The values obtained were corrected for the thermoelectric coefficient of Pt, and a current reversal technique was employed to correct simultaneous four-point conductivity measurements for thermal emf contributions as described by Hong *et al.*[23]

Control of furnace atmosphere was critical to remain in the stability range of $CuAlO_2$. Figure 2 shows the temperature versus $\log pO_2$ phase diagram at 1 atm total pressure for the Cu-Al-O system, using free energies of formation for the various compounds provided by Jacob and Alcock.[24] The line for the $CuAlO_2/CuAl_2O_4/Cu_2O$ equilibrium came from the work of Gadalla and White.[25] In contrast, Jacob and

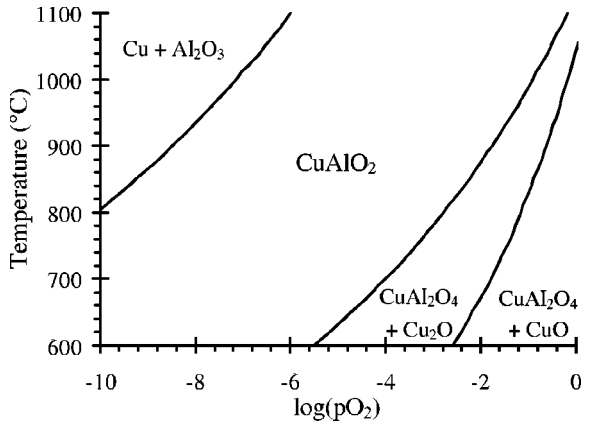


FIG. 2. Temperature vs log $pO_2$ phase diagram for the Cu-Al-O system at 1 atm of total pressure. Thermodynamic data taken from Refs. 24 and 25.

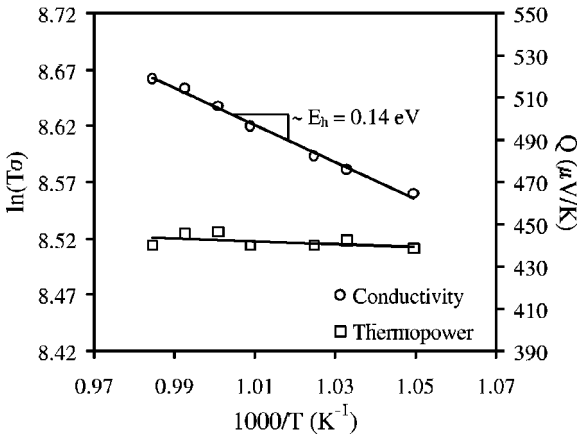


FIG. 3. High-temperature electrical properties for $CuAlO_2$. Range of data taken at $p\ O_2 = 10^{-4}$ atm in Ar balance.

Alcock[24] reported that $CuAlO_2$ was stable all the way to the lower $CuAlO_2/CuAl_2O_4/CuO$ boundary. For both thermodynamic and kinetic reasons (point defect relaxation), measurements were made near or above the upper line under an atmosphere of 100 ppm oxygen in argon. Above 740 °C electrical contacts became unstable, which was also found to occur at lower oxygen partial pressures.

For proper comparison with other experimental results, it was necessary to correct the raw conductivity values for specimen porosity (typically ~60%). This was done using the Bruggeman symmetric model[26] and amounts to a scaling factor of 2.5; all values of conductivity were therefore corrected for porosity by this factor.

To check for grain boundary effects, two-point impedance spectroscopy measurements were made at room temperature using a low-frequency impedance analyzer (Hewlett-Packard 4192A) over the frequency range 5 Hz to 13 MHz with an excitation amplitude of ±1 V.

### B. Theoretical

Electronic structure (and related properties) calculations were carried out with the FLAPW method,[22] which has no shape approximations for the potential and charge density. The exchange-correlation energies were treated within the local-density approximation using the Hedin-Lundqvist[27] parametrization of the exchange-correlation potential. The core states were calculated fully relativistically and updated at each iteration, whereas the valence states were treated semirelativistically. Cutoffs of the plane-wave basis (16.0 Ry) and potential representation (81.0 Ry) and the expansion in terms of spherical harmonics with $l \leqslant 8$ inside the muffin-tin (MT) spheres were used. Summations over the Brillouin zone were done using 28 special $k$ points[28] in the irreducible wedge. The MT-sphere radii (in a.u.) used were 2.0 (Cu), 2.0 (Al), and 1.4 (O). The lattice parameters used for the calculations were fixed with the experimental values $a = 2.8617$ Å and $c = 16.9407$ Å for $CuAlO_2$ measured by x-ray diffraction on bulk material and in excellent agreement with prior results.[5,29]

The optical properties were calculated within the electric-dipole approximation.[30] The imaginary parts of the dielectric functions were thus expressed by

$$\varepsilon_2(\omega) = \frac{8\pi^2 e^2}{\omega^2 m^2 V} \sum_{c,v} \sum_{\mathbf{k}} |\langle c,\mathbf{k}|\hat{\mathbf{e}}\cdot\mathbf{p}|v,\mathbf{k}\rangle|^2 \times \delta[E_c(\mathbf{k}) - E_v(\mathbf{k}) - \hbar\omega], \quad (1)$$

where $c$ and $v$ represent the conduction and valence states, $|n,k\rangle$ are the FLAPW eigenkets, $\mathbf{p}$ is the momentum operator, and $\hat{\mathbf{e}}$ is the unit vector of the external field. The linear tetrahedron scheme[31,32] was employed for the Brillouin Zone integrations using 800 sampling $k$ points in the Brillouin zone. Corrections to the local density approximation (LDA) results, i.e., the underestimation of the band gap, were not employed in obtaining the optical properties.

## III. RESULTS AND DISCUSSION

### A. Electrical properties

The high-temperature electrical properties are shown in Fig. 3. Although the systematic uncertainty is on the order of 5% for both conductivity (due to uncertainty in geometric factors) and thermoelectric coefficient (due to ±1 °C in temperature difference measurements at high temperature),[23] the random error is much smaller, on the order of the symbol size (thermopower) or less (conductivity). This is also seen in the scatter about the fitting lines in each case. Point defect equilibrium was established upon changing temperature and observing the relaxation of the electrical properties, especially the conductivity. Small $pO_2$ excursions were also made, which confirmed the overall $p$-type character of $CuAlO_2$, i.e., the conductivity increased slightly with increasing $pO_2$.

The thermoelectric coefficient was positive ($p$ type) and virtually temperature independent. This indicates that an intrinsic point defect mechanism such as

$$\tfrac{1}{2}O_{2(g)} \rightarrow O_i'' + 2h^{\cdot} \quad (2)$$

is probably not the prevailing mechanism. If it were, we would expect to see a much larger temperature dependence of the thermopower. Either cation off-stoichiometry (Cu/Al $\neq 1$) or tramp impurities (acceptors) set the carrier content.

The fact that the conductivity is thermally activated while the thermopower (hole content) is temperature independent is indicative of small polaron conduction: i.e., the mobility is activated.[8,18] The functional form of the conductivity is[33]

$$\sigma = \frac{\sigma_0}{T} \exp\left( -\frac{E_H}{kT} \right), \tag{3}$$

where $\sigma_0$ is $2.43 \times 10^4$ S K cm$^{-1}$ and the activation or hopping energy is 0.14 eV, as shown in Fig. 3. This value compares favorably with the 0.11–0.23 eV range of prior studies.[4,10–13] Furthermore, the room-temperature value calculated from Eq. (3) is 0.36 S cm$^{-1}$, which compares favorably with previously reported results. The preexponential factor ($\sigma_0$) in Eq. (3) is discussed further below.

The agreement between the room-temperature value calculated using Eq. (3) and the other data in Table I suggests that grain boundaries are *not* a limiting factor in the room-temperature conductivity. To confirm this, two-point impedance spectra were obtained at room temperature. There was a single bulk impedance ($Z$) arc in Nyquist ($-Z_{\text{imaginary}}$ vs $Z_{\text{real}}$) format, whose diameter agreed with four-point dc resistance measurements. Furthermore, its equivalent circuit parameters ($R$,$C$) were consistent with a material of dielectric constant $\sim$10 and overall resistivity consistent with Table I values.

The thermoelectric coefficient for small polaron conductors is given by[34]

$$Q = \pm \frac{k}{e} \ln[2(1-c)/c], \tag{4}$$

where the entropy of transport term has been neglected, $k/e$ is 86.14 $\mu$V/K, and the sign is determined by whether the polaron forms around the trapped electron (negative) or trapped hole (positive). It should be stressed that positive or negative thermopowers can be obtained for either model, being determined by the ratio of available hopping states $(1-c)$ and carriers ($c$). The factor of 2 accounts for spin degeneracy. Based on the experimental thermopower of approximately 440 $\mu$V/K (see Fig. 3), the fraction of $Cu^{2+}$ species can be estimated as $1.21 \times 10^{-2}$ ($Cu^{2+}$ polaron model) or $3.02 \times 10^{-3}$ ($Cu^{+}$ polaron model). Given the overall density of Cu sites ($2.5 \times 10^{22}$ cm$^{-3}$), these values translate into carrier contents of $3.02 \times 10^{20}$ cm$^{-3}$ and $7.56 \times 10^{19}$ cm$^{-3}$, respectively. These values are comparable to those obtained by Gong *et al.*[10] and Yanagi *et al.*[11] and our room-temperature conductivities are also in good agreement.

By combining the hole content (from thermopower) and the conductivity, the high-temperature mobility can be estimated. At 740 °C, the values are 0.1 cm$^2$/V s ($Cu^{2+}$ polaron model) and 0.4 cm$^2$/V s ($Cu^{+}$ polaron model). Both values are consistent with small polaron conduction (typically $<1$ cm$^2$/V s).[34]

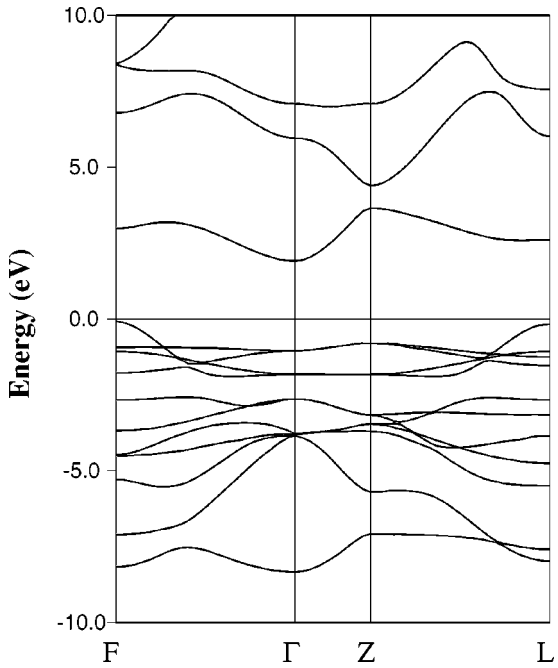


FIG. 4. The self-consistent band structure of $CuAlO_2$ along the high-symmetry directions.

The small polaron analysis can be taken one step further by considering the parameters which make up the preexponential factor $\sigma_0$ in Eq. (3) (Ref. 34):

$$\sigma_0 = \frac{gNc(1-c)e^2a^2\nu}{k}, \tag{5}$$

where $g$ is a geometric factor, $N$ is the density of Cu sites, $c$ and $(1-c)$ are defined above, $e$ is the unit of electron charge, $a$ is jump distance, $\nu$ is the optical phonon frequency responsible for hopping, and $k$ is Boltzmann's constant. The geometric factor is $z/6$, where $z$ is the number of Cu ions surrounding each Cu site (6 in this case) and $a$ is the Cu-Cu distance, taken to be 2.86 Å. Based upon the $\sigma_0$ value of $2.43 \times 10^4$ S K cm$^{-1}$ and the carrier content ($Nc$) estimated from thermopower, optical phonon frequencies of $5.3 \times 10^{12}$ s$^{-1}$ ($Cu^{2+}$ polaron model) and $2.12 \times 10^{13}$ s$^{-1}$ ($Cu^{+}$ polaron model) were estimated, both of which appear to be reasonable values.

### B. Electronic structure

The self-consistent band structure along the high-symmetry directions of the Brillouin zone are shown in Fig. 4. We took the origin of the energies at the valence-band edge at $F$. The high-symmetry points shown in the band structures are $\Gamma(0,0,0)$, $Z(1/2,1/2,1/2)$, $F(1/2,1/2,0)$, and $L(0,1/2,0)$ in terms of the reciprocal basis vectors of the rhombohedral unit cell.[20] While our calculated band structure of $CuAlO_2$ was found to be qualitatively similar to that of the HF calculations,[21] a large important difference can be seen in the lowest conduction band, in particular around $F$ and $L$, where the present calculations show a relatively flat band.

TABLE II. Calculated *l*-decomposed electron charges (in *e*) inside the muffin-tin spheres of $CuAlO_2$ at the valence-band maxima [$F(v)$ and $\Gamma(v)$] and the conduction-band minima [$F(c)$ and $\Gamma(c)$].

| States | Site | *s* | *p* | *d* |
|---|---|---|---|---|
| $F(v)$ | Cu | 0.070 | 0.000 | 1.532 |
| | Al | 0.000 | 0.000 | 0.012 |
| | O | 0.002 | 0.098 | 0.002 |
| $F(c)$ | Cu | 0.000 | 0.390 | 0.000 |
| | Al | 0.000 | 0.018 | 0.000 |
| | O | 0.002 | 0.088 | 0.002 |
| $\Gamma(v)$ | Cu | 0.000 | 0.000 | 1.640 |
| | Al | 0.000 | 0.000 | 0.024 |
| | O | 0.000 | 0.100 | 0.002 |
| $\Gamma(c)$ | Cu | 0.124 | 0.000 | 0.806 |
| | Al | 0.138 | 0.000 | 0.004 |
| | O | 0.158 | 0.046 | 0.002 |

The conduction-band minimum was found at $\Gamma$ and the valence-band maximum at $F$, consistent with the FLAPW results of Yanagi *et al.*[11] The indirect band gap from $F$ to $\Gamma$ was calculated to be 1.95 eV, and the direct optical gap was found to be 2.7 eV. These values compare favorably with the prior FLAPW results of 1.7 eV (indirect) and 2.8 eV (direct),[11] as well as the experimental results of Benko and Koffyberg (1.65 eV for the indirect gap[8]), Yanagi *et al.* (1.8 eV indirect versus 3.5 eV direct)[11] and Kawazoe *et al.* (3.5 eV direct).[1,4] The underestimation of the band gap by the LDA was relatively smaller than the usual values in semiconductors, about 50%. This may result from an error cancellation with an increase of the conduction-band energy around $\Gamma$ because of a self-interaction energy that should be involved in the flat or localized valence bands.[35]

The *l*-decomposed electron charges inside the muffin-tin spheres at $F$ and $\Gamma$ are given in Table II. The conduction-band minima at $\Gamma$ [$\Gamma(c)$] consists mainly of the *s* states and Cu *d* states, which reflects the dispersive bottom of the conduction band. A noticeable mixture with Cu *s* states at $F(v)$ found in Table II and an isotropic charge density in the (001) plane in Fig. 5 [$F(v)$] clearly show the Cu $d_{z^2}$-*s* hybrid orbitals proposed by Orgel.[17] Figure 5 [$F(v)$] also illustrates a linear antibonding structure between Cu $d_{z^2}$-*s* and O $p_z$. On the other hand, the valence bands at $\Gamma(v)$ give the $\pi$-bonding structure with the Cu ($d_{zx}$ and $d_{zy}$) and O ($p_x$ and $p_y$) orbitals as seen in Fig. 5 [$\Gamma(v)$]. The characters at $L$ and $Z$ (not shown) are similar to those at $F$ and $\Gamma$, respectively.

The dispersive features at the topmost valence bands around $F$ (and $L$) will be important for characterizing *p*-type transport properties in $CuAlO_2$ to which hole carriers are introduced. Despite the short Cu-Cu distance (2.86 Å), no dispersion was found along [100] (in the Cartesian coordinate) direction about $F$, suggesting an antibonding interaction between the Cu $d_{z^2}$-*s* hybrid orbitals in this direction.[36] A significant dispersion, with a calculated effective mass of $0.50m_e$, is observed, however, along the [010] direction. This is consistent with a charge density peak existing in this direction, instead of the antibonding structure.[19,21] Bradley and Cracknell[20] calculated the $PdCoO_2$ delafossite structure and found that Pd $d_{z^2}$ orbitals around $F$ and $L$ are the dominant contributions to the states at the Fermi energy and to its metallic conductivity. This metallic state of $PdCoO_2$ was understood by a bonding interaction between unfilled $d_{z^2}$-*s* hybrid orbitals. For a $d^{10}$ ion, such as Cu in $CuAlO_2$, the interaction between the filled $d_{z^2}$-*s* hybrid orbitals is weak, but provides a significant role in the band dispersion,[36] as we observed above. We also emphasize an important contribution to the band dispersion from the linear interaction between Cu $d_{z^2}$-*s* and O$p_z$. To illustrate how the Cu-O distance affects the conductivity, we artificially reduced the lattice parameter, either *a* or *c*, by $-2\%$ and obtained a reduction of the effective mass in the [010] direction around $F$ by $-4.6\%$ or $-3.5\%$, respectively. This strong coupling of the effective mass with the Cu-O distance suggests that hole hopping between copper sites could be enhanced with an assist of the phonon excited by oxygen vibration. These results support the small polaron transport characteristics for the hole hopping observed in the high-temperature electrical property measurements of Fig. 3. The flat valence bands from $\Gamma$ to $Z$ (along [001]) obtained in the band structure (Fig. 4) come from the strongly localized $\pi$-antibonding structure mentioned above and may not contribute to the hole conduc-

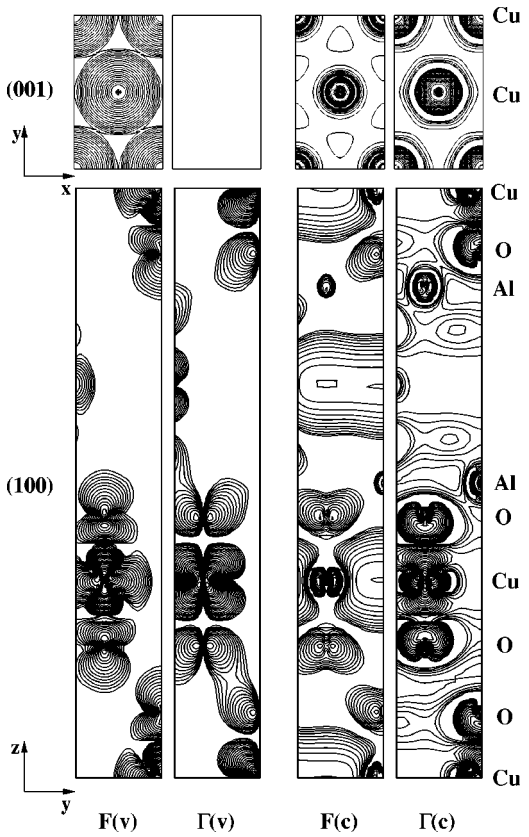


FIG. 5. Electron densities of the valence-band maxima [$F(v)$ and $\Gamma(v)$] and the conduction-band minima [$F(c)$ and $\Gamma(c)$] of $CuAlO_2$ in the (001) plane (the upper figures) and in the (100) plane (the lower figures) where both are passing through the Cu atoms. The contours start from $1\times10^{-3}$ electrons/a.u.$^3$ and change successively by a factor of $\sqrt{2}$.

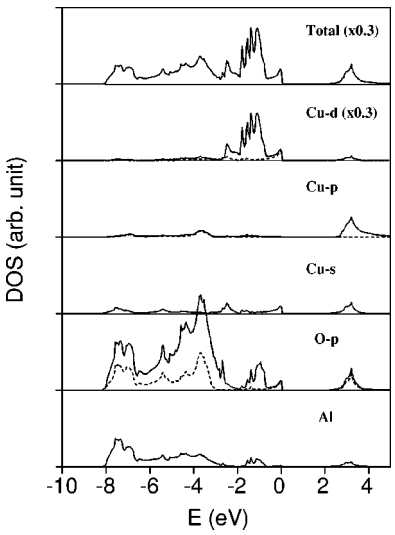


FIG. 6. Total and projected densities of states (DOS) of $CuAlO_2$. The dashed lines for $d$ and $p$ states indicate $d_{z^2}$ and $p_z$ components, respectively.

tivity. This explains the anisotropy (with respect to the $c$ axis) observed in the electrical conductivity.[18]

The DOS presented in Fig. 6 are decomposed into some components to examine the chemical bonding. The valence bands can be divided into three regions: (I) hybridization of Cu $d_{z^2}$-$s$ and O $p_z$ in the topmost valence band, (II) $\pi$ bonding between Cu $d$ and O $p$ states above $-2$ eV to $-0.7$ eV, and (III) $sp$ hybridization bonding between O and Al below $-2$ eV. A sharp edge and the succeeding dispersive feature in region I reflect the anisotropic bonding structures around $F$ discussed above. In the conduction bands below 4 eV, we observed a significant anisotropy in the $p$ states—dominant contributions from Cu $p_x$, Cu $p_y$, and O$p_z$. The Cu $p_x$ and $p_y$ states in the conduction bands form the Cu-Cu interaction as illustrated in Fig. 5 [$F(c)$]. These anisotropic features account for the optical properties through the selection rules described below.

The imaginary parts of the calculated dielectric functions are plotted in Fig. 7. The stacking structure along the $c$ axis of delafossite allows one to evaluate two independent components, the $x/y(E\perp c)$ component (solid lines in the plot), which represents the average over the $x$ and $y$ components, and the $z(E\|c)$ component (dashed lines). The dielectric functions show a significant anisotropy between the $x/y$ and $z$ components. Focusing on each peak observed in the dielectric functions, we examined the corresponding band transitions considered dominant. Peak $A1$ is assigned to transitions from states in region I to the Cu $p_x$ and $p_y$ states in the conduction band around $F$ and $L$, showing the dominant $x/y$ component due to the lack of the $p_z$ component. Peaks $A2$ and $Z1$ are assigned to transitions from the $\pi$ bonding in region II to the Cu $p_x$ and $p_y$ states in the conduction bands. The anisotropy of these transitions is decided by the symmetry of the Cu $t_{2g}$ orbitals in region II. Peak $Z2$ denotes transitions from states in region III to the $s$ states and O $p_z$ states in the conduction band. At the absorption edge, transitions around $\Gamma$ are not optically allowed to a significant degree since there is only a small fraction of $p$ character at $\Gamma(c)$ and $\Gamma(v)$, as in Table II. Therefore, the states belonging to $A1$ do not contribute so much to the absorption edge, and it is expected that replacing $A1$ by another trivalent cation may not significantly change the direct optical absorption edge as long as the lattice parameter of $c$ and thus the Cu-O distance are similar. This is confirmed by a very recent experiment for single-crystal $CuGaO_2$ films,[37] a direct optical band gap was measured to be 3.6 eV, which is quite close to that of $CuAlO_2$ [3.5 eV (Ref. 11)].

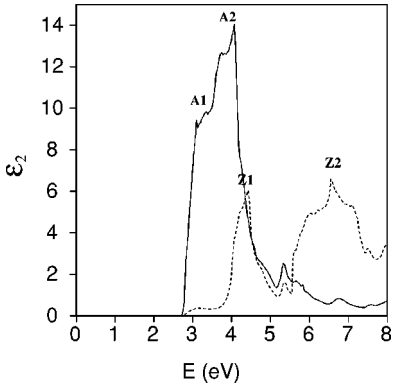


FIG. 7. The imaginary parts of the calculated dielectric functions of $CuAlO_2$ for polarization vectors perpendicular (solid lines) and parallel (dashed lines) to the $c$ axis.

## IV. CONCLUSION

High-temperature electrical property measurements of $CuAlO_2$ offer convincing evidence for small polaron conduction. The electrical conductivity is activated

$$\sigma = \frac{\sigma_0}{T}\exp\left(-\frac{E_H}{kT}\right), \tag{3'}$$

whereas the thermoelectric coefficient is approximately temperature independent. The activation energy obtained is $\sim$0.14 eV. Carrier contents on the order of $10^{19}$–$10^{20}\,\mathrm{cm}^{-3}$ were calculated from the high-temperature thermoelectric coefficient value of $\sim$440 $\mu$V/K. In combination with the electrical conductivity, high-temperature mobilities in the range of 0.1–0.4 $\mathrm{cm}^2/\mathrm{V\,s}$ were calculated, consistent with small polaron transport. The preexponential factor for conductivity ($\sigma_0 = 2.43\times 10^4\,\mathrm{S\,K\,cm}^{-1}$) is consistent with an optical phonon frequency of $\sim 10^{13}\,\mathrm{s}^{-1}$, again consistent with the small polaron model. These data suggest that although substantial carrier content can be obtained in $CuAlO_2$, its mobility will be limited by the small polaron conduction mechanism ($< 1$ $\mathrm{cm}^2/\mathrm{V\,s}$).

The FLAPW method was employed to calculate the band structure, densities of states, and optical properties of $CuAlO_2$. Hybridization between Cu $d_{z^2}$-$s$ and between $d_{z^2}$-$s$ and O $p_z$ are responsible for the dispersion around $F$, while the flat bands from $\Gamma$ to $Z$ in the topmost valence bands, coming from the $\pi$ antibonding between Cu and O, could not contribute to the conductivity. These results are consistent with the two-dimensional small polaron conduction observed

in the present experiment. The optical properties, evaluated within the electric-dipole approximation, show a significant anisotropy with respect to the *c* axis. The strong absorptions at lower energy (<4 eV) come dominantly from transitions with the polarization vector perpendicular to the *c* axis and are mainly due to the two-dimensional Cu *p* states in the conduction band.

**ACKNOWLEDGMENTS**

This work was supported in part under NSF-MRSEC Grant No. DMR-9632472 and under DOE-NREL Contract No. AAD-9-18668-05. B.J.I. was supported by the U.S. Department of Defense.

*Present address: Dept. of Physics, Kookmin University, 86-1, Choungnungdong, Choungnungdong, Songbuk-gu, Seoul 136-702, Korea.

[1] H. Kawazoe, H. Yanagi, K. Ueda, and H. Hosono, Mater. Res. Bull. **25**, 28 (2000).
[2] A. Kudo, H. Yanagi, K. Ueda, H. Hosono, and H. Kawazoe, Appl. Phys. Lett. **75**, 2851 (1999).
[3] H. Ohta, K.-I. Kawamura, M. Orita, M. Hirano, N. Sarukura, and H. Hosono, Appl. Phys. Lett. **77**, 475 (2000).
[4] H. Kawazoe, M. Yasukawa, H. Hyodo, M. Kurita, H. Yanagi, and H. Hosono, Nature (London) **398**, 939 (1997).
[5] R. D. Shannon, D. B. Rogers, and C. T. Prewitt, Inorg. Chem. **10**, 713 (1971).
[6] C. T. Prewitt, R. D. Shannon, and D. B. Rogers, Inorg. Chem. **10**, 719 (1971).
[7] B. U. Kohler and M. Jansen, Z. Anorg. Allg. Chem. **543**, 73 (1986).
[8] F. A. Benko and F. P. Koffyberg, J. Phys. Chem. Solids **45(1)**, 57 (1984).
[9] R. E. Stauber, J. D. Perkins, P. A. Parilla, and D. S. Ginley, Electrochem. Solid-State Lett. **2**, 654 (1999).
[10] H. Gong, Y. Wang, and Y. Luo, Appl. Phys. Lett. **76**, 3959 (2000).
[11] H. Yanagi, S.-I. Inoue, K. Ueda, H. Kawazoe, H. Hosono, and N. Hamada, J. Appl. Phys. **88**, 4159 (2000).
[12] N. Duan, A. W. Sleight, M. K. Jayaraj, and J. Tate, Appl. Phys. Lett. **77**, 1325 (2000).
[13] R. J. Cava, H. W. Zandbergen, A. P. Ramirez, H. Takagi, C. T. Chen, J. J. Krajewski, W. F. Peck, Jr., J. V. Waszczak, G. Meigs, R. S. Roth, and L. F. Schneemeyer, J. Solid State Chem. **104**, 437 (1993).
[14] K. Isawa, Y. Yaegashi, M. Komatsu, M. Nagano, S. Sudo, M. Karppinen, and H. Yamauchi, Phys. Rev. B **56**, 3457 (1997).
[15] K. Isawa, Y. Yaegashi, S. Ogota, M. Nagano, S. Sudo, K. Yamada, and H. Yamauchi, Phys. Rev. B **57**, 7950 (1998).
[16] E. A. Cooper, K. S. Kirkpatrick, B. J. Christensen, B.-S. Hong, and T. O. Mason, in *Grain Boundary Controlled Properties of Fine Ceramics*, edited by K. Ishizaki, K. Nihara, M. Iostani, and R. G. Ford (Elsevier Press, New York, 1992), pp. 3–12.
[17] L. E. Orgel, *An Introduction to Transition-Metal Chemistry: Ligand-Field Theory*, 2nd ed. (Methuen, London, 1966).
[18] D. B. Rogers, R. D. Shannon, C. T. Prewitt, and J. L. Gillson, Inorg. Chem. **10**, 723 (1971).
[19] T. Ishiguro, N. Ishizawa, N. Mizutani, M. Kato, K. Tanaka, and F. Marumo, Acta Crystallogr., Sect. B: Struct. Sci. **39**, 564 (1983).
[20] C. J. Bradley and A. P. Cracknell, *The Mathematical Theory of Symmetry in Solids* (Clarendon, Oxford, 1972).
[21] A. Buljan, P. Alemany, and E. Ruiz, J. Phys. Chem. B **103**, 8060 (1999).
[22] E. Wimmer, H. Krakauer, M. Weinert, and A. J. Freeman, Phys. Rev. B **24**, 864 (1981).
[23] B.-S. Hong, S. J. Ford, and T. O. Mason, Key Eng. Mater. **125–6**, 163 (1997).
[24] K. T. Jacob and C. B. Alcock, J. Am. Ceram. Soc. **58**, 192 (1975).
[25] A. M. M. Gadalla and J. White, J. Br. Ceram. Soc. **63**, 39 (1964).
[26] D. S. McLachlan, M. Blaszkiewicz, and R. E. Newnham, J. Am. Ceram. Soc. **73**, 2187 (1990).
[27] L. Hedin and B. I. Lundqvist, J. Phys. C **4**, 2064 (1971).
[28] H. J. Monkhorst and J. D. Pack, Phys. Rev. B **13**, 5188 (1976).
[29] J. P. Doumerc, A. Wichainchai, M. Pouchard, P. Hagenmüller, and A. Ammar, J. Phys. Chem. Solids **48**, 37 (1987).
[30] P. Y. Yu and M. Cardona, *Fundamentals of Semiconductors* (Springer, Berlin, 1996).
[31] D. Jepson and O. K. Anderson, Solid State Commun. **9**, 1763 (1971).
[32] G. Lehmann and M. Taut, Phys. Status Solidi B **54**, 469 (1972).
[33] H. L. Tuller and A. S. Nowick, J. Phys. Chem. Solids **38**, 859 (1977).
[34] J. Nell, B. J. Wood, S. E. Dorris, and T. O. Mason, J. Solid State Chem. **82**, 247 (1989).
[35] J. P. Perdew and A. Zunger, Phys. Rev. B **23**, 5048 (1981).
[36] A. Buljan, M. Llunell, E. Ruiz, and P. Alemany, Chem. Mater. **13**, 338 (2001).
[37] K. Ueda, T. Hase, H. Yanagi, H. Kawazoe, H. Hosono, H. Ohta, M. Orita, and M. Hirano, J. Appl. Phys. **89**, 1790 (2000).